ELSEVIER

Journal of Power Sources 81–82 (1999) 340–345

JOURNAL OF POWER SOURCES

www.elsevier.com/locate/jpowsour

Electrochemical impedance spectroscopy study of SnO and nano-SnO anodes in lithium rechargeable batteries

Hong Li, Xuejie Huang, Liquan Chen *

Laboratory for Solid State Ionics, Institute of Physics, Chinese Academy of Sciences, P.O. Box 603, Beijing 100080, China

Abstract

Nano-SnO and normal SnO anodes for lithium rechargeable batteries have been investigated by electrochemical impedance spectroscopy (EIS). Three types of equivalent circuits have been used to fit the spectra at different discharge states. The variations of impedance spectra, charge-transfer resistance and double layer capacitance have been discussed. The electrochemical reaction mechanism of SnO anode for lithium ion batteries can be deduced as follows: a passivating film forms on the surface of SnO particles firstly, then Li^+ ions pass through the surface film and react with SnO to produce amorphous Li_2O and to form fine grains of Li–Sn alloys in the core region underneath the passivating film.

Keywords: SnO anodes; Nanometer anodes; Impedance spectroscopy; Passivating film

1. Introduction

Recently, oxide anodes for lithium rechargeable batteries have drawn great attention due to their large reversible capacity [1]. A two-step reaction mechanism of tin oxides with lithium was proposed and confirmed by considering the results of in-situ XRD, Raman and HRTEM [2–4]. Lithium first reacts irreversibly with oxide to produce amorphous Li_2O and Sn, then Sn alloys with Li and forms different Li–Sn alloys. Here, the first reaction step is named as replacement reaction, the second step as alloy reaction.

The microstructure of nano-SnO at deep discharged state was studied by HRTEM [4]. On the surface of SnO particles, a perfect shell-like structure was clearly observed. Underneath the shell structure, a lot of Li–Sn alloy crystallites were dispersed into amorphous Li_2O matrix. This shell structure was supposed as the solid electrolyte interface (SEI), which was caused by the electrolyte decomposition reaction. The composition of the SEI was analyzed by FTIR [5]. The peaks of Li_2CO_3 and $ROCO_2Li$ were identified. It was found that Li_2CO_3 appeared above 0.9 V vs. Li/Li^+ (1.2–0.9 V), while $ROCO_2Li$ could be observed mainly below 0.9 V. This scenario means that Li_2CO_3 is formed firstly, then followed by $ROCO_2Li$. Furthermore, Raman spectra confirmed that the replacement reaction of SnO occurs above 0.9 V [5].

In a previous work, it was found that only one broad irreversible peak presented in the cyclic voltammogram of SnO anode at the first cycle [6]. This peak ranged from 1.2 to 0.4 V vs. Li/Li^+, then followed another reduction peak ranged from 0.4 to 0.0 V, which should attribute to alloy reaction. Considering all results, it may be concluded that the replacement reaction and the formation of SEI occur firstly, then followed by alloy reactions.

However, it is still difficult to decide the reaction sequence between replacement reaction and decomposition reaction based on above results. Two possibilities may be existed. The first one, a passivating film forms on the surface of SnO particles, then Li^+ ions pass through the surface film and react with SnO to form amorphous Li_2O and Li_xSn in the core regions. The second possibility is that SnO particles firstly react with lithium and decompose into small particles which are composed of Li_2O and Sn. Then, the passivating film forms on the surface of these small particles, following alloy reaction. The first case is named as M1 mechanism for short, the second one is called M2 mechanism. Any of them may have significant but different influence on the electrochemical properties of SnO anodes. In this work, nano-SnO and normal SnO anodes at several discharged states were investigated by electrochemical impedance spectroscopy (EIS). A detail reaction mechanism is discussed based on the results.

* Corresponding author. Fax: +86-10-62562605; E-mail: lqchen@aphy02.iphy.ac.cn

0378-7753/99/$ - see front matter
PII: S0378-7753(99)00214-1

2. Experimental

Nano-scale SnO powders (100 nm) were obtained by mechanical ball milling normal SnO (250 meshes) for 12 h under an argon atmosphere using agate balls in the shearing mode. The weight ratio of balls to sample powder was 4:1.

EIS measurements were carried out using a sealed three-electrode ground-glass cell. The working electrode was a typical pressed-powder electrode [7]. It was prepared by pasting the slurries of normal SnO or nanometer SnO powder, carbon black and polyvinylidene fluoride (PVDF) dissolved in cyclopentanone onto a nickel grid. After pasting, the electrodes were dried at 120°C for 8 h under vacuum and were compressed at 1×10^7 Pa between two stainless steel plates. The weight ratio of SnO to carbon black and PVDF is 85:10:5. The counter and reference electrodes were pure lithium foils. The electrolyte was 1 M $LiPF_6$ dissolved in ethyl carbonate (EC) and diethyl carbonate (DEC) (1:1 in volume). The cells were assembled in an argon-filled glove box. The cells were discharged to different depth at a constant current density of 0.1 mA/cm^2, then were kept for 22 h for equilibrium.

Impedance measurements were performed using a Solartron 1174 frequency response analyzer coupled with a 1186 electrochemical interface under the control of an Apple IIe computer. The cells were shielded and kept thermostatically at 25 ± 0.1°C during measurements. Data were collected over the frequency ranging from 1 mHz to 10 kHz with 5 mV ac oscillation. EIS data was analyzed by the EQUIVCRT 3.91 program developed by Boukamp [8].

3. Results and discussion

The electrochemical reactions presented in metal oxide anode are more complicated than carbon anodes or intercalation cathodes. The following processes should be considered when SnO anode is discharged in the first cycle:

(a) Electrochemical reactions:

$Li^+ + SnO + e^- \rightarrow Sn + Li_2O$ (1)

$Li^+ + Sn + e^- \rightarrow Li_xSn$ ($x \leq 4.4$) (2)

$Li^+ + (EC, DEC, \ldots) + e^- \rightarrow$ SEI (Li_2CO_3, $ROCO_2Li$, $\ldots$) (3)

(b) Diffusion processes:

Li^+ ions diffusion in pore electrolyte within the pores of anode (4)

Li^+ ions diffusion within matrix of anode (5)

(c) Phase transitions:

The formation of surface layer (6)

The replacement reaction of SnO (7)

The formation of different Li_xSn alloys (8)

Crack and crumb of product particles (9)

According to previous work, processes (1), (3), (4), (6), and (7) occurred first, then the other processes would be followed. If these processes have different time constants, it is possible to distinguish them in impedance spectrum.

In order to improve resolution, our previous experiments, include FTIR, Raman and HRTEM were carried out mainly based on nano-SnO anode. Here, the impedance spectrum of normal SnO and nano-SnO at different discharge states were compared at the same time to avoid possible interference caused by particle size. The discussion was divided into four sections.

3.1. General description to the EIS of SnO and nano-SnO anodes

The impedance spectra of SnO anode at different discharged states are shown in Fig. 1. The inset figure is the zoom part at the range of high frequency. At the original state, the SnO anode exhibited a typical behavior of the blocking electrode as shown in Fig. 1(1), spectrum 1. After the cell was discharged to a capacity of 65 mAh/g, it could be observed clearly from the spectrum 2 in Fig. 1(1) that a new semicircle appeared in the middle frequency range. In general, the presence of the second semicircle indicates a typical response of grain interior–grain boundary phase systems [9]. Since the existence of the passivating film on the surface of nano-SnO anode has been confirmed by HRTEM and FTIR [4,5]. Thus, the new semicircle should be assigned to the formation of SEI film. An inclined line was also observed from the spectrum 2 in the low frequency regions. It may be related to the process (4) since Li^+ ions may not diffuse into SnO lattice at this discharged depth. It was found that the diameter of high frequency semicircle increased before the cell was discharged to the capacity of 372 mAh/g (see Fig. 1(2)). Thereafter, two semicircles were merged into one semicircle. This variation may imply that new interface disappears and the anode transforms into a homogeneous structure. The diameter of the combined semicircle at high frequencies increased with the deepening of discharge as indicated in Fig. 1(2). However, the impedance of the SnO anode at low frequencies increased from spectrum 5 to spectrum 6, then decreased at spectrum 7 and spectrum 8 in Fig. 1(2).

The EIS behaviors of nano-SnO anode are similar with normal SnO anode. But the variation of impedance spectra with the discharged depth is more obvious than that of normal SnO anode. The emerging process of the second semicircle is very clear (see spectrum 2 and spectrum 3 in Fig. 2(1)). Then the second semicircle was a little indistinct at the discharge depth of 380 mAh/g, and merged with high frequency semicircle at the depth of 428 mAh/g (see spectrum 4 in Fig. 2(1), and spectrum 5 in Fig. 2(2)). It is very clear from spectrum 6 and spectrum 7 in Fig. 2(2) that the diameter of the high frequency semicircle decreased firstly and increased again.

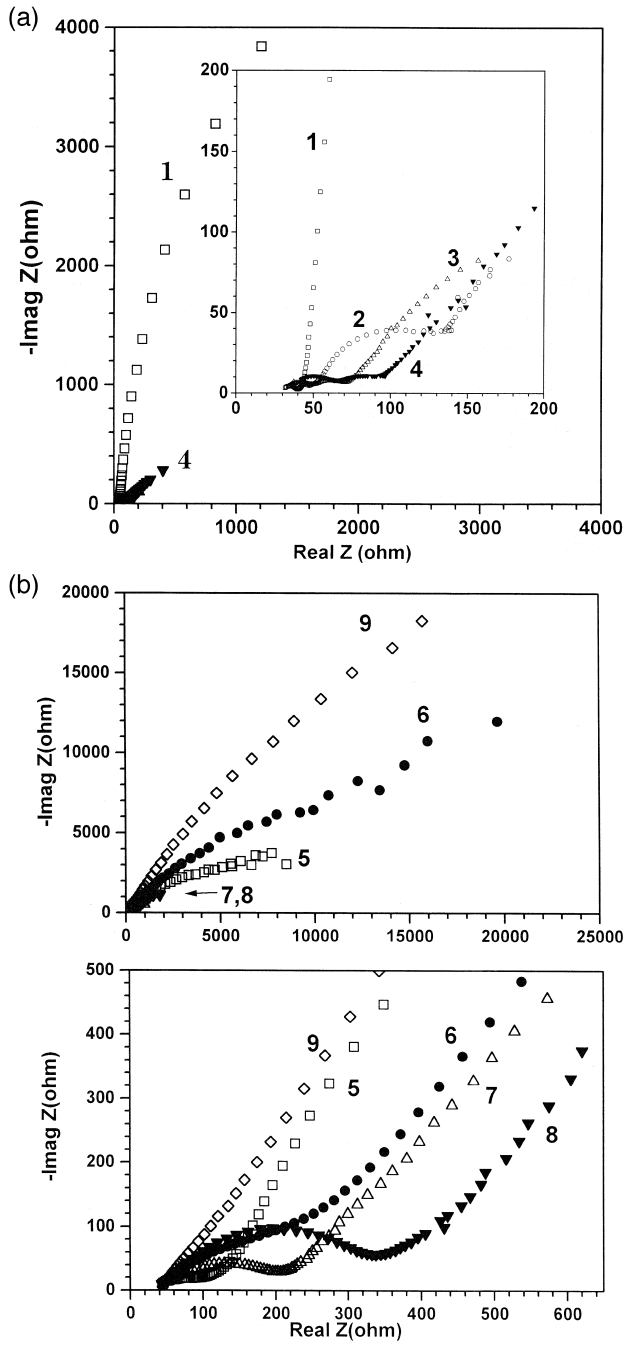

Fig. 1. (a) Impedance spectra of normal SnO anode at different discharge states in a three-electrode lithium cell: SnO/1 M $LiPF_6$, EC–DEC (1:1)/Li/Li. (A) Whole frequencies range, (B) zoom part at high frequencies region. (1) 3.186 V, OCV; (2) 2.761 V, 65 mAh/g; (3) 2.755 V, 152 mAh/g; (4) 2.749 V, 261 mAh/g. (b) Impedance spectra of normal SnO anode at different discharge states in a three-electrode lithium cell: SnO/1 M $LiPF_6$, EC–DEC (1:1)/Li/Li. (5) 1.827 V, 372 mAh/g; (6) 0.975 V, 415 mAh/g; (7) 0.763 V, 502 mAh/g; (8) 0.417 V, 546 mAh/g, then shorted; (9) 2.683 V, charged.

At charged state, the EIS behaviors for both normal SnO anode and nano-SnO anode are similar. The response at whole frequencies may be regarded as an imperfect semicircle shown in spectrum 9 in Fig. 1(2) and spectrum 8 in Fig. 2(2). It may indicate that the anode at charged state has larger polarization resistance which may be caused by a larger interface impedance and charge accumulation on the surface of the anode.

3.2. Equivalent circuits for EIS

Three types of equivalent circuit (EC) were used to fit the impedance spectra of SnO anode at different discharge states shown in Fig. 3. The constant-phase element (CPE) was used in EC due to the dispersion effect. EC1 describes EIS with one semicircle and a linear part. R_S is uncompensated ohmic resistance. R_{ct} is charge-transfer resistance, Q_1 is double layer capacitance (C_{dl}) of the electrode–electrolyte interface. Q_2 at original state (correspondent to spectrum 1 in both Figs. 1 and 2) represents a capacitance related to blocking electrode. However, at discharged states (correspondent to spectrum 7 and spectrum 8 in Fig. 1(2) and spectrum 5, spectrum 6 and spectrum 7 in Fig. 2(2)). Q_2 represents a semi-infinite diffusion impedance (Wurburg impedance).

EC2 describes EIS with two semicircles and a linear part (spectrum 2, spectrum 3 and spectrum 4 in both Figs. 1(1) and 2(1)). Q_1 and Q_2 are in parallel with R_{el} and R_{film} and represent C_{dl} and capacitance of surface film (C_{film}), respectively. Q_3 is related to the diffusion impedance.

EC3 describes EIS with two semicircles (spectrum 5 and spectrum 6 in Fig. 1(2)). The second semicircle may be considered as a charge accumulation process caused by a slow interface process in which guest ions incorporate from the electrolyte into the electrode lattice. This phenomenon is more common in the case of intercalation electrode, which can be described by a C_{ad} in parallel with $R_{lattice}$ [10,11] to describe this charge accumulation process. Q_1 also represents C_{dl}.

3.3. Results and analysis to the equivalent circuit elements

Fig. 4 plotted the variation of R_{ct} vs. discharge capacity for normal SnO and nano-SnO anodes. The black ellipse dots in right inset figure represent the R_{ct} values of SnO and nano-SnO anodes at charged state. The variation tendency of R_{ct} is same for both anodes. R_{ct} increases firstly with the deepening of discharge, then drops to a lower point and rises again. The variation of C_{dl} is in opposite to R_{ct} shown in Fig. 5, the black ellipse dots is the C_{dl} value of SnO and nano-SnO at charged state.

Charge-transfer resistance is not only related to the redox reaction existing on the surface of electrodes, but also affected by the structure of electrode. Based on mechanism M2, when SnO anode is discharged, SnO particles are decomposed into many smaller particles composed of

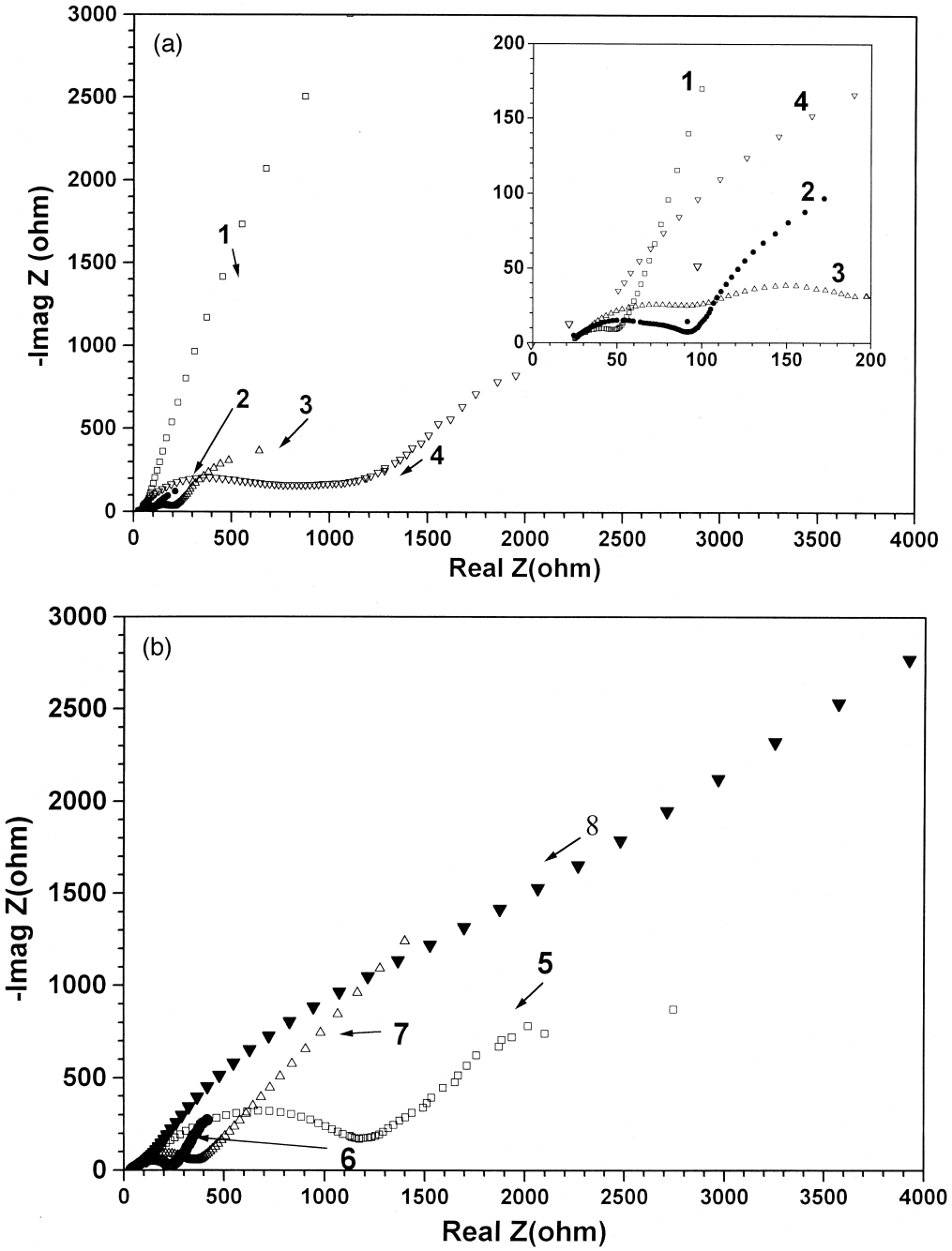

Fig. 2. (a) Impedance spectra of nano-SnO anode at different discharge states in a three-electrode lithium cell: nano-SnO/1 M $LiPF_6$, EC–DEC (1:1)/Li/Li. (A) Whole frequencies range, (B) zoom part at high frequencies region. (1) 3.105 V, OCV; (2) 2.737 V, 95.6 mAh/g; (3) 2.718 V, 222 mAh/g; (4) 2.635 V, 380 mAh/g. (b) Impedance spectra of nano-SnO anode at different discharge states in a three-electrode lithium cell: nano-SnO/1 M $LiPF_6$, EC–DEC (1:1)/Li/Li. (A) Whole frequencies range, (B) zoom part at high frequencies region. (5) 2.545 V, 428 mAh/g; (6) 0.591 V, 619 mAh/g; (7) 0.428 V, 714 mAh/g, then, shortcut; (8) charged to 1.904 V, 430 mAh/g.

Li_2O and metal Sn. The R_{ct} should not increase since more active reaction sites and conductive Sn atoms are produced with the deepening of discharge. While according to the mechanism M1, with the thickening of the surface film, the charge transfer process should become more difficult. It will lead to the increasing of R_{ct}. When the anode is discharged to a certain depth, the formation of SEI is not predominant, more and more lithium ions pass through the surface film and produce Li–Sn alloys, the charge transfer process may become easier. At charged state, the de-insertion of lithium ions may decrease the conductivity of ions and electrons. The charge transfer will become more difficult. Thus, the variation of R_{ct} at various discharged states is consistent with mechanism M1.

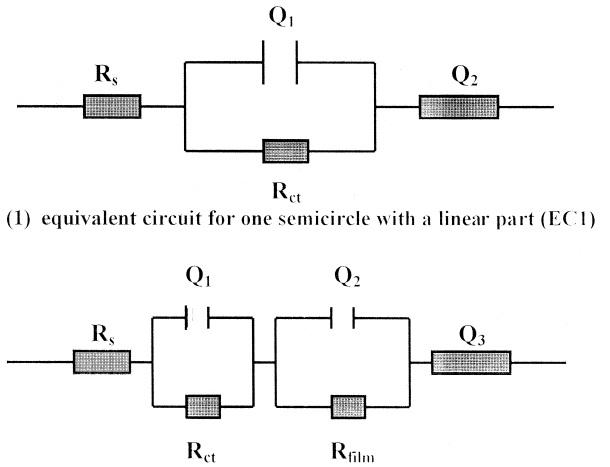

Fig. 3. Equivalent circuits used for fitting the impedance spectra of SnO anode R_s: ohmic resistance, R_{ct}: charge-transfer resistance, Q: constant phase element, R_{film}: resistance of surface film, $R_{lattice}$: incorporation of ions into lattice.

C_{dl} is proportional to the surface area and permittivity of the electrode material and inverse proportional to the thickness of electrical double layer. Based on the mechanism M2, the surface area will increase since original SnO particles are decomposed into small particles. However, the formation of a perfect surface film will not cause notable increasing of the surface area of the anode. Thus, the variation of C_{dl} supports mechanism M1.

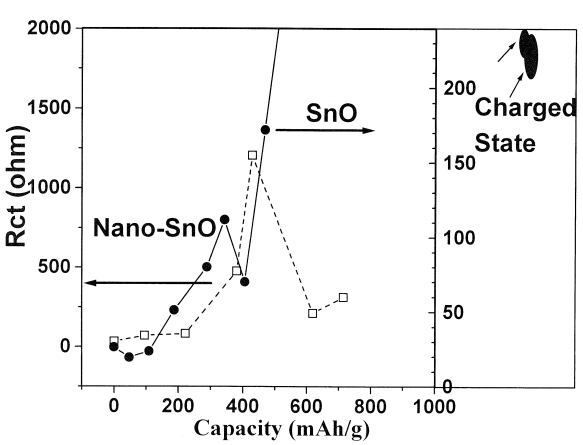

Fig. 4. R_{ct} of normal SnO and nano-SnO anodes at different discharge states.

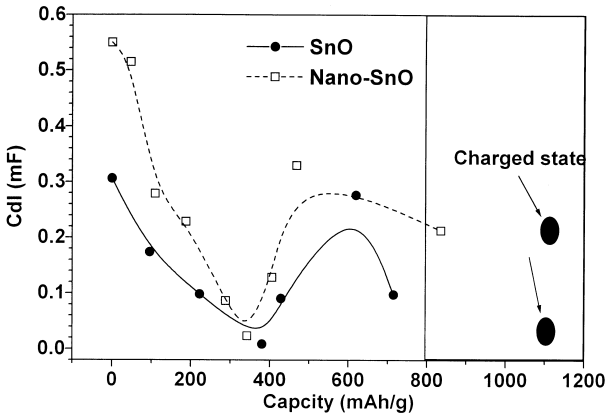

Fig. 5. C_{dl} of normal SnO and nano-SnO anodes at different discharge states.

3.4. A model for the insertion process of lithium ions into SnO lattice

It is obvious from above analysis to the impedance spectra that mechanism M1 is more reasonable. A simple model of SnO anode during the insertion process of lithium ions was shown in Fig. 6 based on M1 mechanism. Due to the formation of the surface film at shallow discharged states, two semicircles were presented in the impedance spectra for both normal SnO and nano-SnO anode. One is attributed to the interface between the surface film and the electrolyte, another is related to the interface between the surface film and inner SnO lattice (state 2 in Fig. 6). With the deepening of discharge, the surface film is thickened and the crystal structure of SnO is destroyed gradually and transferred into disorder matrix (state 3 in Fig. 6). As a result, the boundary between the surface film and the crystal of SnO becomes obscure gradually. Finally, the boundary disappears and forms a continuous disorder structure. Thus, two semicircles are merged into one semicircle in impedance spectra.

It has been confirmed according to the results of in-situ XRD, Raman and cyclic voltammogram, that SnO and SnO_2 have the same two-step reaction mechanism with lithium [2,3,5,6,12]. The microstructure of SnO_2 anode at a shallow discharged state was investigated by HRTEM [13]. It was found that a disorder surface layer covered on the surface of SnO_2. Underneath the surface film, the crystal stripes of SnO_2 can be seen clearly and still kept completely. At deep discharged state, the boundary between surface film and crystal disappeared. Furthermore, from the HRTEM images of the SnO anode at deep discharged state [4], it was found that the surface film also has a disorder structure. The boundary between surface film and core region is not very sharp. Thus, the presence and disappear of this boundary are confirmed by TEM. Therefore, all experimental results are consisted with mechanism M1.

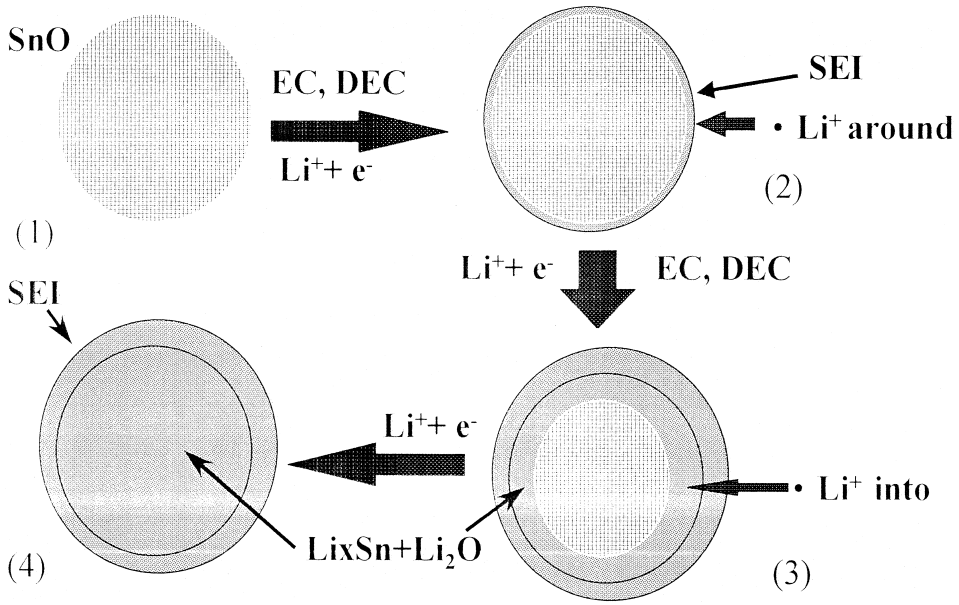

Fig. 6. The reaction model of SnO anode after inserting with lithium ions in nonaqueous electrolyte. (1) Original state. (2) Initial discharged state, the surface film begin to form. (3) Intermediate discharged state, the surface film is thickening and the replacement reaction begins. (4) Deep discharged state, alloy reaction terminate.

It should be noted that the influence of the particle size to the variation of impedance spectra is not obvious, the double layer capacitance for nano-SnO anode is only two times higher than normal SnO anode. This indicates that real surface area may not equal to the electrochemical active area, if the anode was prepared by pressing the powder.

4. Conclusions

The impedance spectra of normal SnO anode and nano-SnO anode have been investigated at different discharge states in 1 M $LiPF_6$, EC–DEC (1:1). Combined with previous results of FTIR, Raman and HRTEM, the electrochemical reaction mechanism of SnO anode for lithium ion batteries can be deduced as follows.

Firstly, organic solvents are reduced and react with Li ions to form a passivating film (SEI) on the surface of SnO anode. Next, Li^+ ions pass through the SEI film and react with SnO. The crystal structure of SnO is destroyed and fine Li_2O and metal Sn particles are produced and interspersed. Then Sn atoms alloy with Li^+ ions to form different Li–Sn alloy depending on the content of insert Li^+ ions. With the evolution of the reactions, the boundary between surface film and crystal structure disappears.

Acknowledgements

This work was supported by Ford-NSFC Foundation (contract no. 9712304), NSFC (contract no. 59672027) and National 863 Key Program (contract no. 715-004-0280).

References

[1] Y. Idota, T. Kubota, A. Matsufuji, Y. Maekawa, T. Miyasaka, Science 276 (1997) 1395.
[2] I.A. Courtney, J.R. Dahn, J. Electrochem. Soc. 144 (1997) 2045.
[3] W.F. Liu, X.J. Huang, Z.X. Wang, H. Li, L.Q. Chen, J. Electrochem. Soc. 145 (1998) 59.
[4] H. Li, X.J. Huang, L.Q. Chen, Electrochem. Solid-State Lett. 1 (1998) 241.
[5] H. Li, J.Z. Li, Z.X. Wang, X.J. Huang, L.Q. Chen, submitted.
[6] H. Li, X.J. Huang, L.Q. Chen, Solid State Ionics, in press.
[7] M.G.S.R. Thomas, P.G. Bruce, J.B. Goodenough, J. Electrochem. Soc. 132 (1985) 1521.
[8] B.A. Boukamp, Solid State Ionics 20 (1986) 31.
[9] N. Bonanos et al., in: J.R. Macdonald (Ed.), Impedance Spectroscopy, Chap. 4, Wiley, 1987, p. 198.
[10] P.G. Bruce, M.Y. Saidi, Solid State Ionics 51 (1992) 187.
[11] H. Li, Z. Lu, H. Huang, X. Huang, L. Chen, Ionics 2 (1996) 259.
[12] T. Brousse, R. Retoux, U. Herterich, D.M. Schleich, J. Electrochem. Soc. 145 (1998) 1.
[13] W.F. Liu, The study of anode-related materials of lithium ion battery, PhD Thesis, Institute of Physics, Chinese Academy of Sciences, 1997.